Characterization of the two-photon transition phase in the buildup process of Rabi oscillations

Xu Zhang,[1] Yijie Liao,[1] Yongkun Chen,[1] Miao Yu,[1] Kunlong Liu,[1] Peixiang Lu,[1,2] and Yueming Zhou[1,*]

[1]*School of Physics and Wuhan National Laboratory for Optoelectronics, Huazhong University of Science and Technology, Wuhan 430074, China*

[2]*Optics Valley Laboratory, Hubei 430074, China*

(Received 14 November 2023; accepted 25 January 2024; published 1 March 2024)

We achieve the complete characterization of the transition phase in the resonant two-photon ionization (TPI) of hydrogen at the high laser intensity where Rabi oscillation occurs. Different from previous studies which focused on the transition phase of resonant TPI in the perturbation region, in our work, we reveal the effect of Rabi oscillations on the transition phase in the high-intensity region. With bichromatic extreme-ultraviolet light, the transition phases of the S and D partial waves are decoded. By solving the time-dependent Schrodinger equation, we show that the transition phase depends on not only the pulse duration but also the laser intensity. This dependence is traced back to the modification of the atomic state structure, rather than the competition between resonant and nonresonant ionization paths at the lower laser intensity. Our work provides a way to manipulate the two-photon transition phase through laser intensity.

DOI: 10.1103/PhysRevA.109.033101

I. INTRODUCTION

Photoionization is a fundamental process in the light-matter interaction, in which two-photon ionization (TPI) and multiphoton ionization [1–3] enabled by the development of high-harmonic generation and free-electron lasers [4–7] have attracted intensive interest. Currently, various attosecond techniques, such as streaking [8,9] and reconstruction of attosecond beating by interference of two-photon transitions (RABBIT) [10–19], have been widely applied to measure the quantum phase of the photoelectrons, which has provided fundamental insight into the dynamics of the photoionization. This has led to a renewed interest in characterization of the phase in the TPI process, especially for the resonance TPI. In the far-off-resonance region, the ionized electron wave packet is unstructured, and the measured phase can be divided into the Wigner scattering phase determined by the energy and the angular momenta of the initial and final states [20–25] and the continuum-continuum transition phase [26,27]. However, in the near-resonant region, the two-photon ionization process via a resonance gives rise to an additional phase, the so-called transition phase. This transition phase is the manifestation of the target electronic structure and the ionization-path competition [28,29]. Its pulse duration and energy detuning dependence have been theoretically studied [30,31] and have been experimentally observed with single extreme-ultraviolet (XUV) pulses [28,29,32–34], as well as the RABBIT technique [10–12,14,15,17,18,35]. However, due to the intensity limitations of the laser source, previous studies focused on the lower-laser-intensity region, where the results of the transition phase can be described with the lowest-order perturbation theory.

Very recently, with the seeded free-electron laser providing intense XUV laser sources, Autler-Townes (AT) doublets [36–41] were observed in the resonant TPI of He [42]. This splitting in the energy spectra is a manifestation of Rabi oscillation during photoionization. The transition from unsplit to split energy spectra represents the buildup of Rabi oscillations [36–41,43]. Due to the occurrence of Rabi oscillations, the photoelectron wave packets are structured, and their phases are significantly affected by the phase introduced by the oscillating populations of the initial state, and most importantly, the behavior of the two-photon transition phase is very different from that of the lower-laser-intensity region. The transition phase is sensitive to atomic properties, which are perturbed due to the intense laser field, and the occurrence of Rabi oscillations. Therefore, it is worthwhile to reveal how the buildup process of Rabi oscillations modulates the two-photon transition phase.

In this work, we investigate the behavior of the two-photon ionization transition phase during the buildup of the Rabi oscillations by numerically solving the time-dependent Schrödinger equation (TDSE). We employ bichromatic laser fields to decode the transition phases for the S and D partial waves from the total phase of the electron wave packets. The bichromatic-electric-field method, which allows for the complete characterization of phases, was recently utilized in various experiments [44–50]. This method employs two phase-locked XUV pulses with frequencies ω and 2ω and is now available in free-electron laser facilities and has become an important tool for characterizing the electron phase in photoionization. Here, we employ these bichromatic laser fields to reveal the transition phases of different partial waves in resonant TPI. In the low-intensity region before the onset of Rabi oscillations, the transition phases of the S and D partial waves are asymptotic towards zero from opposite directions with increasing pulse duration. As the laser

*zhouymhust@hust.edu.cn

intensity increases, the transition phase smoothly varies from 0 to -0.5π for both partial waves due to the onset of Rabi oscillation. As the laser intensity or pulse duration further increases, the AT splitting in the photoelectron energy spectrum appears. We analyzed the transition phase for the lower- and higher-energy peaks in doublets. The difference between their transition phases moves from a nontrivial value to π. Our analysis indicates that in the high-intensity region, the nonresonant states affect the transition phase by modifying the atomic state structure, rather than through direct competition with the resonant ionization path in the low-intensity region [28]. Additionally, the splitting of the initial state introduces additional modifications to the atomic state structure, exerting further impact on the transition phases. To further validate our analysis, we employ a dressed-level model [51,52]. Our results suggest that the two-photon transition phases can be manipulated through laser intensity.

II. METHODS

The photoelectron momentum distributions (PEMDs) are obtained by numerically solving the three-dimensional TDSE [53] of the hydrogen atomic system in the velocity gauge.

The TDSE is written (in atomic units) as

$$i\frac{\partial\psi(\mathbf{r},t)}{\partial t} = H(\mathbf{r},t)\psi(\mathbf{r},t), \tag{1}$$

where

$$H(\mathbf{r},t) = -\frac{1}{2}\nabla^2 - \frac{1}{r} - i\mathbf{A}(t)\cdot\nabla. \tag{2}$$

Here, the purely time-dependent quadratic $\frac{1}{2}A(t)^2$ term has been removed by the gauge transformation $\psi' = \exp[i\int_{-\infty}^{t}\frac{1}{2}A^2(t)dt]$. $\mathbf{A}(t)$ is the vector potential of bichromatic laser fields in the dipole approximation, written as the sum of the laser fields ω and 2ω:

$$\mathbf{A}(t) = A_\omega \sin^2\left(\frac{\omega t}{2N}\right)\sin(\omega t)\mathbf{e}_z + A_{2\omega}\sin^2\left(\frac{\omega t}{2N}\right)\sin(2\omega t+\gamma)\mathbf{e}_z, \tag{3}$$

where $A_{\omega(2\omega)}$ is the amplitude of the vector potential of the laser field ω (2ω) and N is the number of the optical cycles, which characterizes the pulse duration. γ is the relative phase between the ω and 2ω fields. $g(t) = \sin^2(\frac{\omega t}{2N})$ is the pulse envelope. The intensity of the field 2ω is 2 orders of magnitude smaller than that of the field ω.

The TDSE in Eq. (1) is solved in the spherical coordinates, where the wave function is expanded by the spherical harmonics $|l,m\rangle$, $\psi(\mathbf{r},t) = \sum_{l,m}\frac{R_{lm}(r,t)}{r}|l,m\rangle$. Here, $R_{lm}(r,t)$ is the radial part of the wave function, which is discretized by the finite-element discrete-variable-representation method [54]. The time propagation of the TDSE is calculated by the split-Lanczos method [55] with a time step of $\Delta t = 0.01$ a.u. In each step of the propagation, we split the wave function $\psi(\mathbf{r},t)$ into the inner part $\psi_{\rm in}(\mathbf{r},t) = \psi(\mathbf{r},t)F_{\rm sp}$ and the outer part $\psi_{\rm out}(\mathbf{r},t) = \psi(\mathbf{r},t)(1-F_{\rm sp})$, where $F_{\rm sp} = 1 - (1+e^{(R-R_c)/d})^{-1}$ is the absorbing mask function. The inner part $\psi_{\rm in}(\mathbf{r},t)$ evolves as the TDSE in Eq. (1), and $\psi_{\rm out}(\mathbf{r},t)$ is propagated by a Coulomb-Volkov propagator [56] and then projected to the scattering state to obtain the ionization amplitudes.

In our numerical simulations, the maximal box size $R_{\rm max}$ for radial coordinates is $R_{\rm max} = 1000$ a.u. The absorbing boundary R_c is 800 a.u., with $d = 2$ a.u. The number of partial waves is chosen to be $L_{\rm max} = 10$, which ensures convergence of the calculations.

III. NUMERICAL RESULTS AND DISCUSSION

We calculate the photoionization of hydrogen by the bichromatic laser fields with frequencies $\omega = 0.375$ a.u. and $2\omega = 0.75$ a.u. The ω field is resonant with the $1s$ and $2p$ states of hydrogen. The hydrogen atom is ionized by absorbing two ω photons or one 2ω photon. For the resonant TPI process induced by the ω laser field, there are two outgoing partial waves, S ($|\psi_s\rangle$) and D ($|\psi_d\rangle$). The amplitudes for the S and D partial waves are expressed as

$$\begin{aligned} a_s &= \sum_m \int dt \frac{1}{i}E_\omega(t)\langle\psi_s|z|\psi_m\rangle e^{i(E_f-E_m)t} \\ &\quad\times\int_{-\infty}^{t}dt'\frac{1}{i}E_\omega(t')\langle\psi_m|z|\psi_I\rangle e^{i(E_m-E_I)t'}a_I(t'), \\ a_d &= \sum_m \int dt \frac{1}{i}E_\omega(t)\langle\psi_d|z|\psi_m\rangle e^{i(E_f-E_m)t} \\ &\quad\times\int_{-\infty}^{t}dt'\frac{1}{i}E_\omega(t')\langle\psi_m|z|\psi_I\rangle e^{i(E_m-E_I)t'}a_I(t'), \end{aligned} \tag{4}$$

where I and m represent the initial and intermediate states, respectively, and E_I and E_m are their energies. E_f corresponds to the energy of the final continuum state. Two-photon continuum-continuum transitions via an intermediate state are ignored in Eq. (4) due to their low probability [51,52]. For the single-photon ionization from the 2ω laser field, the final state

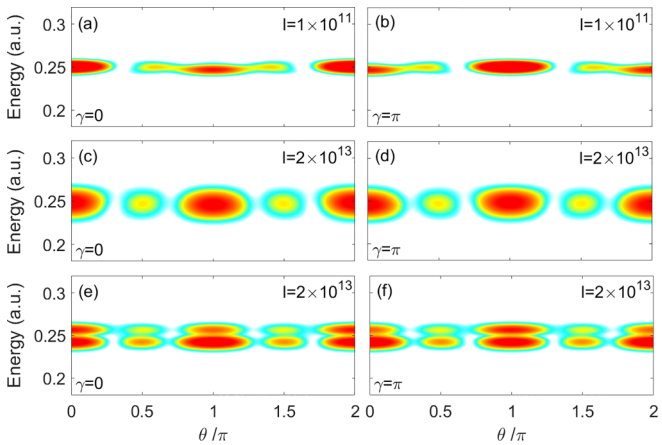

FIG. 1. (a) and (b) PEMDs at a laser intensity of 1×10^{13} W/cm^2 and pulse duration $N = 60$. (c) and (d) PEMDs at a laser intensity of 2×10^{13} W/cm^2 and pulse duration $N = 30$. (e) and (f) PEMDs at a laser intensity of 2×10^{13} W/cm^2 and pulse duration $N = 60$. The relative phase of the two fields is $\gamma = 0$ in the left column and $\gamma = \pi$ in the right column. θ is the angle between the electron emission direction and the polarization direction of the laser fields.

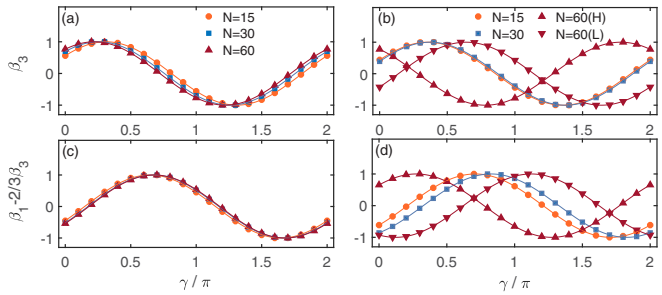

FIG. 2. Normalized β_3 and $\beta_1 - \frac{2}{3}\beta_3$ as a function of the relative phase γ at laser intensities of (a) and (c) 1×10^{11} W/cm^2 and (b) and (d) 2×10^{13} W/cm^2. The orange circles, blue squares, and red triangles denote the results for pulse durations $N = 15$, 30, and 60, respectively.

is the P partial wave $|\psi_p\rangle$, serving as a reference for probing the phases of the S and D waves. The amplitudes for the P partial waves are expressed as

$$a_p = \int dt \frac{1}{i} E_{2\omega}(t)\langle\psi_p|z|\psi_I\rangle e^{i(E_f - E_I)t} a_I(t). \tag{5}$$

Figure 1 displays the PEMDs at different laser intensities and pulse durations. At the low laser intensity where Rabi oscillations have not yet begun, the PEMD presents a single-peak structure [Figs. 1(a) and 1(b)]. At the higher laser intensity of 2×10^{13} W/cm^2, Rabi oscillations occur. The PEMD still displays the single-peak structure at a pulse duration of $N = 30$ [Figs. 1(c) and 1(d)]. This is because the atom suffers approximately one Rabi period and the AT splitting has not built up yet [42]. As the pulse duration increases, AT doublets appear in the PEMD, as shown in Figs. 1(e) and 1(f). Furthermore, the PEMDs depend on the relative phase γ between the two-color fields, as indicated in the left and right columns of Fig. 1.

The relative phase γ dependence of the PEMDs can be expressed with the partial coherence method [57],

$$I(\theta) = ||a_p|e^{i(\eta_p - \pi + \phi_I - \gamma)}Y_{10}(\theta,\varphi) + |a_s|e^{i(\eta_s - \frac{\pi}{2} + \phi_s + \phi_I)} \times Y_{00}(\theta,\varphi) + |a_d|e^{i(\eta_d - \frac{3\pi}{2} + \phi_d + \phi_I)}Y_{20}(\theta,\varphi)|^2, \tag{6}$$

where a_p, a_s, and a_d are the amplitudes of the partial waves and θ is the polar angle of the photoelectron with respect to the polarization direction of the laser field. $\eta_{s,p,d}$ represent the Wigner phase, and the extra phase ϕ_I is introduced by the oscillating populations of the initial state $a_I(t)$, which are identical for all three partial waves. $\phi_{s(d)}$ denotes the two-photon transition phase of S (D) partial wave. This phase appears due to the presence of the (near-)resonant state in the finite pulse and reflects the atomic properties in the presence of a laser pulse. In previous studies [28,29], the angular distribution of photoelectrons in a single-color XUV pulse was analyzed to extract the difference in transition phases between different partial waves at a laser intensity within the perturbation region. In this work, we analyze the transition phases ϕ_s and ϕ_d in the high-intensity region where Rabi oscillations can occur.

Equation (6) can be expanded as a series of Legendre polynomials $P_l(\theta)$:

$$I(\theta) = \beta_0 P_0(\theta) + \beta_1 P_1(\theta) + \beta_2 P_2(\theta) + \beta_3 P_3(\theta) + \beta_4 P_4(\theta). \tag{7}$$

The asymmetry parameters β_n are determined as a function of a_p, a_s, and a_d as follows:

$$\begin{aligned}
\beta_0 &= \frac{1}{4\pi}(|a_p|^2 + |a_s|^2 + |a_d|^2),\\
\beta_1 &= \frac{1}{4\pi}\left\{\frac{4}{5}\sqrt{15}|a_d||a_p|\cos\left[\gamma + \left(\eta_d - \eta_p + \phi_d - \frac{\pi}{2}\right)\right] + 2\sqrt{3}|a_p||a_s|\cos\left(\gamma + \left[\eta_s - \eta_p + \phi_s + \frac{\pi}{2}\right)\right]\right\},\\
\beta_2 &= \frac{1}{4\pi}\frac{1}{7}[10|a_d|^2 + 14\sqrt{5}|a_d||a_s|\cos(\eta_d - \eta_s + \phi_d - \phi_s - \pi) + 14|a_p|^2],\\
\beta_3 &= \frac{1}{4\pi}\frac{6}{5}\sqrt{15}|a_d||a_p|\cos\left[\gamma + \left(\eta_d - \eta_p + \phi_d - \frac{\pi}{2}\right)\right],\\
\beta_4 &= \frac{1}{4\pi}\frac{18}{7}|a_d|^2,\\
\left(\beta_1 - \frac{2}{3}\beta_3\right) &= \frac{1}{4\pi}2\sqrt{3}|a_p||a_s|\cos\left[\gamma + \left(\eta_s - \eta_p + \phi_s + \frac{\pi}{2}\right)\right].
\end{aligned} \tag{8}$$

We employ β_3 and $(\beta_1 - \frac{2}{3}\beta_3)$ to determine the transition phase $\phi_{s(d)}$. The results of β_3 and $(\beta_1 - \frac{2}{3}\beta_3)$ extracted from the PEMDs as a function of the relative phase γ are shown in Fig. 2. Figures 2(a) and 2(c) display the results obtained at a low laser intensity of 1×10^{11} W/cm^2, where Rabi oscillations do not occur. A small phase shift occurs in both the β_3 and $(\beta_1 - \frac{2}{3}\beta_3)$ curves with increasing pulse duration. Figures 2(b) and 2(d) show the results obtained at a higher laser intensity of 2×10^{13} W/cm^2, where Rabi oscillations do occur. For the short pulse durations, the AT splitting has not shown up in the PEMDs (the corresponding results are marked with orange circles and blue squares). As the pulse duration increases, there is also a small phase shift in both the β_3 and $(\beta_1 - \frac{2}{3}\beta_3)$ curves. Additionally, both the β_3 and

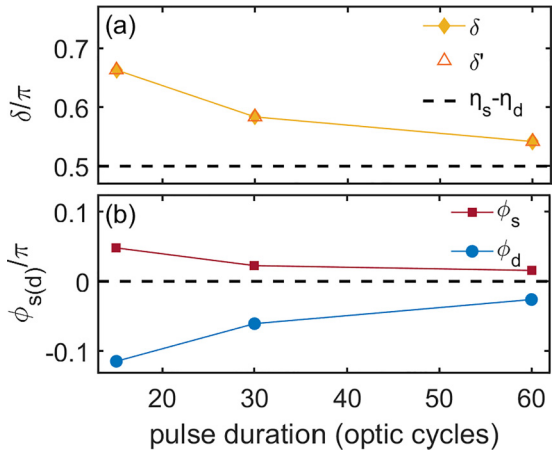

FIG. 3. (a) Phase difference $\delta = (\phi_s + \eta_s) - (\phi_d + \eta_d)$ (yellow diamonds) as a function of pulse duration. For comparison, the results calculated by the method in [28,29] are plotted as open orange triangles (δ'). The dashed horizontal lines denote the Wigner phase difference $\eta_s - \eta_d$. (b) The transition phases ϕ_s (red squares) and ϕ_d (blue circles) as a function of pulse duration. The laser intensity is 1×10^{11} W/cm^2.

$(\beta_1 - \frac{2}{3}\beta_3)$ curves show a phase shift compared to the low-intensity case [shown in Figs. 2(a) and 2(c)]. As the pulse duration increases to $N = 60$, the AT doublets appear in the PEMDs (the corresponding results are marked with red triangles). We extract both β_3 and $(\beta_1 - \frac{2}{3}\beta_3)$ from the higher- and lower-energy peaks in the doublets. The curves for the higher- and lower-energy peaks in the doublets (labeled H and L, respectively) display distinct and opposite phase shift compared to the low-intensity case [shown in Figs. 2(a) and 2(c)].

We extract the phases $\phi_s + \eta_s - \eta_p$ and $\phi_d + \eta_d - \eta_p$ by fitting $(\beta_1 - \frac{2}{3}\beta_3)$ and β_3 with cosine functions. Figure 3 illustrates the obtained phases in the low-intensity region (1×10^{11} W/cm^2), where Rabi oscillations do not occur. Figure 3(a) displays the phase differences $\delta = (\phi_s + \eta_s) - (\phi_d + \eta_d)$ as a function of pulse duration (yellow diamonds). As the pulse duration increases, the phase difference δ gradually approaches the Wigner phase difference $\eta_s - \eta_d$. This indicates that the value of $\phi_s - \phi_d$ approaches zero with increasing pulse duration. For comparison, we also obtain this phase difference by analyzing the angular distribution of the photoelectrons in the single-color XUV pulses. The excellent agreement between the two methods confirms that the phase perturbations introduced by probing laser pulse 2ω in the proposed method are negligible. We then retrieve the transition phase of each partial wave $\phi_{s(d)}$ by subtracting the Wigner phases $\eta_s - \eta_p$ and $\eta_d - \eta_p$ [58–60]. The results as a function of the pulse duration are shown in Fig. 3(b). The signs of the transition phases ϕ_s (red squares) and ϕ_d (blue circles) are opposite; both vary gradually with the pulse duration and approach zero in the long-limit pulse. In this low-intensity region, without rapid population exchange between the initial and resonant states, the lowest-order perturbation theory is applicable [17]. The expression for the final-state amplitude in the resonant TPI is given by

$$\tilde{a}_f = \frac{1}{i}\int_{-\infty}^{+\infty} d\omega \tilde{E}_\omega(\omega_{mI})\tilde{E}_\omega(\omega_{fI} - \omega_{mI}) \times \sum_m \frac{\langle\psi_f|z|\psi_m\rangle\langle\psi_m|z|\psi_I\rangle}{E_I - E_m + \omega + i\Gamma}, \tag{9}$$

where ω_{mI} and ω_{fI} are transition frequencies connecting the initial ($|\psi_I\rangle$) and intermediate ($|\psi_m\rangle$) states and the initial and final ($|\psi_f\rangle$) states, respectively. The term Γ originates from the finite pulse duration and is proportional to the spectral width of the ω pulse [12,13,30]. The transition phase $\phi_{s(d)}$ can be expressed as the sum of the contributions from the resonant state ($|\psi_R\rangle$) and the nonresonant states ($|\psi_n\rangle$),

$$\phi_{s(d)} = \mathrm{Arg}\left[i\frac{\mu_{s(d)R}\mu_{RI}}{E_I - E_R + \omega + i\Gamma} + \sum_n i\frac{\mu_{s(d)n}\mu_{nI}}{E_I - E_n + \omega + i\Gamma}\right], \tag{10}$$

where $\mu_{s(d)R} = \langle\psi_{s(d)}|z|\psi_R\rangle$, $\mu_{RI} = \langle\psi_R|z|\psi_I\rangle$, $\mu_{s(d)n} = \langle\psi_{s(d)}|z|\psi_n\rangle$, and $\mu_{nI} = \langle\psi_n|z|\psi_I\rangle$ are the transition dipole matrix elements between the continuum and resonant states, the resonant and initial states, the continuum and nonresonant states, and the nonresonant and initial states, respectively. The energy detuning from the resonance $E_I - E_R + \omega$ is zero. As indicated by Eq. (10), in the low-intensity case without Rabi oscillations, the transition phase from the resonant state (the first term) is zero for both S and D waves. Therefore, the opposite signs of the S and D transition phases are attributed to the different contributions of the nonresonant states contained in the ionization paths for the S and D waves (the second term). Moreover, the dependence of the transition phase on the pulse duration is related to the term Γ, which is proportional to the spectral width of the ω pulse. As the pulse duration increases, the relative contribution of the nonresonant states to the transition phase gradually decreases [28]. Thus, the transition phases ϕ_s and ϕ_d are asymptotic towards zero, and the phase-shift difference δ is approximately the Wigner phase difference $\eta_s - \eta_d$.

As the laser intensity increases, Rabi oscillations occur. Figures 4 and 5 display the pulse duration and intensity dependence of the transition phase $\phi_{s(d)}$ in this high-intensity region. Figure 4 shows the pulse-duration dependence of the transition phases ϕ_s (red squares) and ϕ_d (blue circles) at a laser intensity of 2×10^{13} W/cm^2. Figure 4(a) shows the transition phases at short pulse durations where the AT splitting has not yet shown up in the PEMDs. The phases ϕ_s and ϕ_d vary from 0 to -0.5π as the pulse duration increases from $N = 15$ to $N = 45$. When the pulse duration exceeds $N = 60$, AT splitting appears in the PEMDs, and then we separately extract the transition phases for the higher- and lower-energy peaks in the doublets, as shown in Fig. 4(b) (labeled H and L, respectively). It is shown that the transition phase of the higher-energy peak gradually increases to 0.5π with increasing pulse duration and decreases to -0.5π for the lower-energy peak. Correspondingly, with increasing pulse duration, the phase differences between the AT doublets

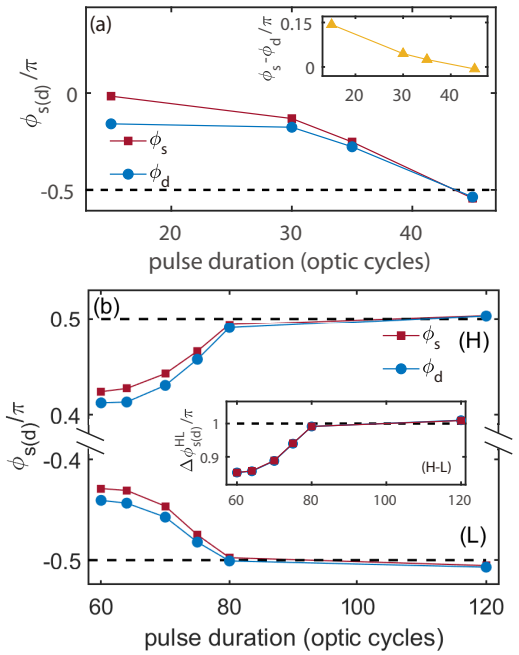

FIG. 4. Transition phases ϕ_s (red squares) and ϕ_d (blue circles) as a function of the pulse duration. In (a), the AT doublets have not shown up in the photoelectron energy spectrum. In (b), the AT doublets have shown up, and the results for the higher- and lower-energy peaks in the doublets are separately displayed (labeled by H and L, respectively). The inset in (a) shows the phase difference between ϕ_s and ϕ_d. The inset in (b) illustrates the phase difference between the AT doublets. The laser intensities in all panels are 2×10^{13} W/cm^2. The dashed horizontal lines located at -0.5π, 0.5π, and π are added to guide the eye.

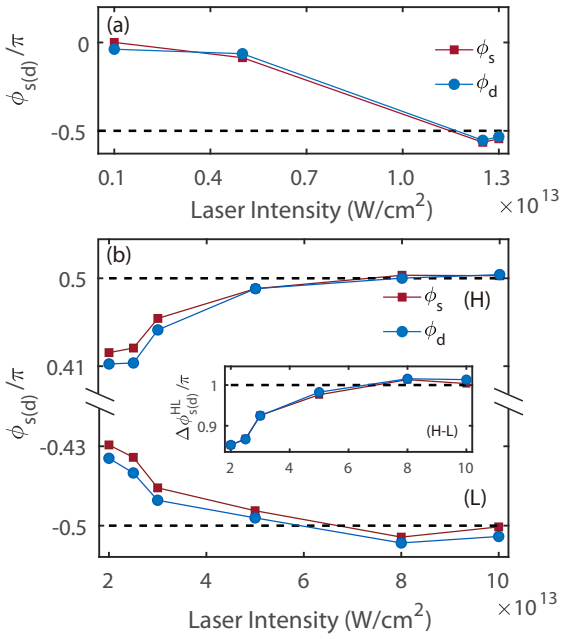

FIG. 5. Transition phases ϕ_s (red squares) and ϕ_d (blue circles) as a function of laser intensity. In (a), the AT doublets have not shown up in the photoelectron energy spectrum. In (b), the AT doublets have shown up, and the results for the higher- and lower-energy peaks in the doublets are separately displayed (labeled by H and L, respectively). The inset in (b) illustrates the phase difference between the AT doublets. The pulse duration is $N = 60$ for all panels. The dashed horizontal lines are added to guide the eye.

(labeled H-L) increase to π [shown in the inset of Fig. 4(b)], as expected for an infinite pulse duration. Additionally, Fig. 4 shows that the phase difference between ϕ_s and ϕ_d is smaller compared to that in the low-intensity case.

Figure 5 displays the intensity dependence of the transition phases ϕ_s (red squares) and ϕ_d (blue circles) for a pulse duration of $N = 60$. Figure 5(a) shows the transition phases for intensities lower than 1.3×10^{13} W/cm^2; in this regime, the AT splitting has not yet shown up in the PEMDs. The phases ϕ_s and ϕ_d gradually decrease to -0.5π as the laser intensity increases. When the laser intensity exceeds 2×10^{13} W/cm^2, AT splitting appears in the PEMDs. The corresponding transition phases of the higher- and lower-energy peaks in doublets are shown in Fig. 5(b) (labeled H and L, respectively), and their differences are shown in the inset of Fig. 5(b) (denoted by H-L). It is shown that, as the laser intensity increases, the transition phase of the higher-energy peak gradually increases to 0.5π and decreases to -0.5π for the lower-energy peak. Correspondingly, with increasing laser intensity, the transition-phase differences between the AT doublets (H-L) increase from 0.85π to π. Additionally, Fig. 5 shows that ϕ_s and ϕ_d are almost the same in this region.

Figures 4 and 5 reveal distinct differences in transition phases between intensity regions where Rabi oscillations occur and do not occur. The transition phases are influenced not only by the pulse duration but also by the laser intensity. The observed phenomena arise from modifications introduced to the atomic state structures by the intense laser field. In the case depicted in Figs. 4(a) and 5(a) where the AT splitting has not built up, the strong coupling to nonresonant states in this higher-intensity region leads to significant ac Stark shifts in the states $|\psi_I\rangle$ and $|\psi_R\rangle$ and the final state $|\psi_f\rangle$ and subsequently modifies the transition phase [in Eq. (10)] to

$$\phi_{s(d)} = \mathrm{Arg}\left[i \frac{\mu_{s(d)R}\mu_{RI}}{\tilde{E}_I - S_f - E_R + \omega + i\Gamma} + \sum_n i \frac{\mu_{s(d)n}\mu_{nI}}{\tilde{E}_I - S_f - E_n + \omega + i\Gamma} \right]. \quad (11)$$

Here, $\tilde{E}_I = E_I + S_I$, where S_I is the ac Stark shift of the initial state. S_f refers to the energy shift of the final state and is approximately equal to U_p. The transition phase from the resonant state (the first term) is no longer zero. The direct contribution from the nonresonant states to the transition phase (the second term) is negligible compared to that of the resonant state. Therefore, in the high-intensity region, the nonresonant states primarily affect the transition phase by modifying the atomic state structure rather than directly contributing to it (i.e., through direct competition with the resonant ionization path as observed in the low-intensity region). This results in the smaller phase difference between the S and D waves, as shown in Figs. 4 and 5, as well as the shift

of the S-wave transition phase from positive to negative, in contrast to the low-intensity case (shown in Fig. 3). The value of Γ decreases with increasing pulse duration. Additionally, the absolute value of $\tilde{E}_I - S_f - E_R + \omega$ increases with increasing laser intensity. Consequently, the transition phase $\phi_{s(d)} \approx \mathrm{Arg}[i\frac{\mu_{s(d)R}\mu_{RI}}{\tilde{E}_I - S_f - E_R + \omega + i\Gamma}]$ decreases as the pulse duration or laser intensity increases, as shown in Figs. 4(a) and 5(a).

AT splitting appears in the PEMDs upon further increasing the pulse duration or laser intensity, as illustrated in Figs. 4(b) and 5(b). The strong coupling between the initial state $|\psi_I\rangle$ and the resonant state $|\psi_R\rangle$ causes the initial state to split into two quasieigenstates,

$$\tilde{a}_I(t) = \frac{\Delta\tilde{\omega} + \tilde{\Omega}}{2\tilde{\Omega}} e^{i(\frac{1}{2}\Delta\tilde{\omega} - \frac{1}{2}\tilde{\Omega})t} + \frac{-\Delta\tilde{\omega} + \tilde{\Omega}}{2\tilde{\Omega}} e^{i(\frac{1}{2}\Delta\tilde{\omega} + \frac{1}{2}\tilde{\Omega})t}. \tag{12}$$

Here,

$$\tilde{\Omega}(t) \cong \sqrt{[\mu_{RI}E_0 g(t)]^2 + [\Delta\tilde{\omega}(t)]^2} \tag{13}$$

is the effective Rabi frequency. E_0 and $g(t)$ are the amplitude and the envelope of the electric field, and $\Delta\tilde{\omega} = \omega - \omega_{\tilde{R}I}$ denotes the photon energy detuning between the shifted initial and resonant states (where $\omega_{\tilde{i}\tilde{j}} = \tilde{E}_i - \tilde{E}_j$ and $\tilde{E}_i = E_i + S_i$). The amplitudes of the final states for the higher- and lower- energy doublets are expressed as

$$\tilde{a}_{f_\pm} = \frac{1}{2i}\left(\frac{\pm\Delta\tilde{\omega} + \tilde{\Omega}}{2\tilde{\Omega}}\right)\int_{-\infty}^{+\infty} d\omega\tilde{E}_\omega\left(\omega_{m\tilde{I}} + \frac{1}{2}\Delta\tilde{\omega} \mp \frac{1}{2}\tilde{\Omega}\right)\tilde{E}_\omega \times (\omega_{\tilde{f}I} - \omega_{m\tilde{I}})\sum_m \frac{\langle\psi_f|z|\psi_m\rangle\langle\psi_m|z|\psi_I\rangle}{\tilde{E}_I - \frac{1}{2}\Delta\tilde{\omega} \pm \frac{1}{2}\tilde{\Omega} - S_f - E_m + \omega + i\Gamma}. \tag{14}$$

Compared to Eq. (11), it is shown that the splitting of the initial state (due to the strong coupling with resonant state) introduces additional modifications $-\frac{1}{2}\Delta\tilde{\omega} \pm \frac{1}{2}\tilde{\Omega}$ to the atomic state structure, which exerts further impact on the transition phases. The transition phases for the higher- and lower-energy peaks in doublets are expressed as $\phi_{s(d)+} \approx \mathrm{Arg}[i\frac{\mu_{s(d)R}\mu_{RI}}{\tilde{E}_I - \frac{1}{2}\Delta\tilde{\omega} + \frac{1}{2}\tilde{\Omega} - S_f - E_R + \omega + i\Gamma}]$ and $\phi_{s(d)-} \approx \mathrm{Arg}[i\frac{\mu_{s(d)R}\mu_{RI}}{\tilde{E}_I - \frac{1}{2}\Delta\tilde{\omega} - \frac{1}{2}\tilde{\Omega} - S_f - E_R + \omega + i\Gamma}]$, respectively. Hence, the opposite signs of the transition phases for the AT doublets are due to the $\pm\frac{1}{2}\tilde{\Omega}$ terms. The value of Γ decreases with increasing pulse duration. Additionally, the absolute value of $\tilde{E}_I - \frac{1}{2}\Delta\tilde{\omega} \pm \frac{1}{2}\tilde{\Omega} - S_f - E_R + \omega$ (primarily determined by the $\frac{1}{2}\tilde{\Omega}$ term) increases with increasing laser intensity. As a result, the transition phases $\phi_{s(d)}$ approach $\pm\frac{\pi}{2}$ with increasing pulse duration or laser intensity, as shown in Figs. 4(b) and 5(b). Furthermore, the phase difference between the AT doublets [shown in the insets of Figs. 4(b) and 5(b)] is not precisely equal to a unit of π. This is the result of the combined effects of the pulse width and the shifting and splitting of energy states induced by the Rabi oscillations.

Finally, we numerically solve the dressed-level model derived from Eq. (14), containing the $1s$, $2p$, $3p$, and $4p$ states:

$$\tilde{a}_f = \sum_{m=2p,3p,4p}\frac{1}{2i}\left(\frac{\pm\Delta\tilde{\omega} + \tilde{\Omega}}{2\tilde{\Omega}}\right)\int_{-\infty}^{+\infty} d\omega\tilde{E}_\omega \times \left(\omega_{m\tilde{1}s} + \frac{1}{2}\Delta\tilde{\omega} \mp \frac{1}{2}\tilde{\Omega}\right)\tilde{E}_\omega(\omega_{f\tilde{1}s} - \omega_{m\tilde{1}s}) \times \frac{\langle\psi_f|z|\psi_m\rangle\langle\psi_m|z|\psi_{1s}\rangle}{\tilde{E}_{1s} - \frac{1}{2}\Delta\tilde{\omega} \pm \frac{1}{2}\tilde{\Omega} - S_f - E_m + \omega + i\Gamma}. \tag{15}$$

The ac Stark shifts of $|\psi_I\rangle$ and $|\psi_R\rangle$ and the final state $|\psi_f\rangle$ are $S_I = \sum_n[\mu_{\mathrm{in}}\frac{1}{2}E_0 g(t)]^2\frac{2\omega_{\mathrm{in}}}{\omega_{\mathrm{in}}^2 - \omega^2} \approx -0.7E_0^2$, $S_R = \sum_n[\mu_{Rn}\frac{1}{2}E_0 g(t)]^2\frac{2\omega_{Rn}}{\omega_{Rn}^2 - \omega^2} \approx 2.6E_0^2$, and $S_f = U_p \approx \frac{E_0^2}{4\omega^2}$, respectively [52]. The simulated results ϕ_s (light red squares) and ϕ_d (light blue circles) as a function of laser intensity are displayed in Fig. 6. These results successfully reproduce the dependence of the transition phase on laser intensity (as demonstrated in Fig. 5). Furthermore, we calculate the transition phase ϕ_R (open green triangles) by including only the resonant state $2p$ for comparison. Their agreement reaffirms that the direct contribution from nonresonant states to the transition phase is negligible. In the high-intensity region, the behavior of the transition phase is primarily attributed to modifications to the atomic state structure, rather than the competition between resonant and nonresonant paths, as observed in the low-intensity region [28]. Moreover, all modifications to the atomic structure, that is, the terms $S_{I,R,f}$, $\pm\frac{1}{2}\tilde{\Omega}$, and $\Delta\tilde{\omega}$, exhibit a direct dependence on the laser intensity.

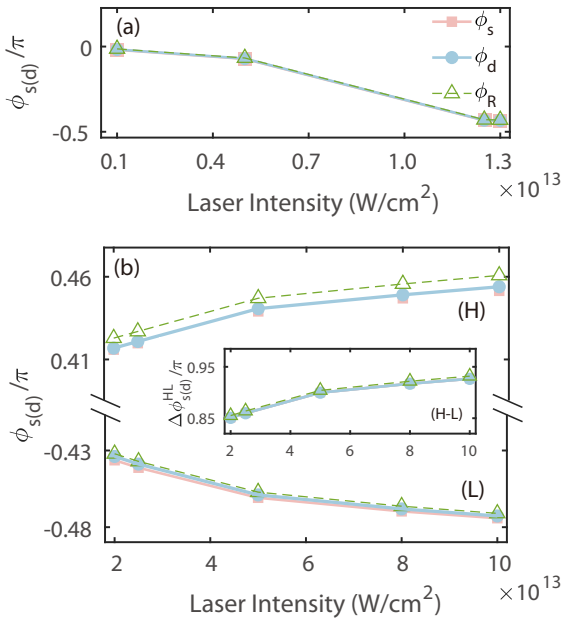

FIG. 6. Transition phases ϕ_s (light red squares) and ϕ_d (light blue circles) obtained from the dressed-level model [Eq. (15)]. The laser parameters are the same as those in Fig. 5. The open green triangles represent the results where only the resonant state $2p$ is considered. In this case, the transition phases for the S and D partial waves are exactly the same.

This dependence suggests the possibility of modulation of the two-photon transition phase through the manipulation of laser intensity.

IV. CONCLUSIONS

We theoretically studied the behaviors of the transition phases in the resonant TPI process during the buildup of the Rabi oscillations. Bichromatic laser fields were applied to access the transition phases for the S and D partial waves, respectively.

In the low-intensity region before the onset of Rabi oscillations, the transition phases ϕ_s and ϕ_d are asymptotic towards zero from opposite directions as the pulse duration increases. This behavior arises from the different contributions of nonresonant states to the transition phases of S and D partial waves and becomes negligible in the long-pulse region. As the laser intensity increases, the Rabi oscillations occur, and the behaviors of transition phases are distinctly different from those in the low-intensity region. The transition phases are influenced not only by the pulse duration but also by the laser intensity. This is due to the modification introduced in atomic state structures by the intense laser field. Consequently, the nonresonant states primarily affect the transition phase by modifying the atomic state structure (via the resultant ac Stark shifts), rather than through direct competition with the resonant ionization path, as observed in the low-intensity region. Furthermore, the splitting of the initial state introduces additional modifications to the atomic state structure, exerting further impact on the transition phases. Our work provides the possibility of manipulating transition phases in resonant TPI processes through laser intensity. Although precisely controlling the laser intensity is difficult in experiment due to the unavoidable focal-intensity volume average effect, the dependence of the transition phase on laser intensity should still be observable, where the intensity can be considered the effective intensity due to the average of the atom ensemble in the focal volume.

ACKNOWLEDGMENTS

This work was supported by the National Key Research and Development Program of China (Grant No. 2019YFA0308300) and the National Natural Science Foundation of China (Grant No. 12374264). The computing work in this paper was supported by the Public Service Platform of High Performance Computing provided by the Network and Computing Center of Huazhong University of Science and Technology (HUST).

[1] N. Miyamoto, M. Kamei, D. Yoshitomi, T. Kanai, T. Sekikawa, T. Nakajima, and S. Watanabe, Observation of two-photon above-threshold ionization of rare gases by XUV harmonic photons, Phys. Rev. Lett. **93**, 083903 (2004).

[2] H. Hasegawa, E. J. Takahashi, Y. Nabekawa, K. L. Ishikawa, and K. Midorikawa, Multiphoton ionization of He by using intense high-order harmonics in the soft-x-ray region, Phys. Rev. A **71**, 023407 (2005).

[3] M. Kretschmar, A. Hadjipittas, B. Major, J. Tümmler, I. Will, T. Nagy, M. J. J. Vrakking, A. Emmanouilidou, and B. Schütte, Attosecond investigation of extreme-ultraviolet multi-photon multi-electron ionization, Optica **9**, 639 (2022).

[4] W. Ackermann *et al.*, Operation of a free-electron laser from the extreme ultraviolet to the water window, Nat. Photon. **1**, 336 (2007).

[5] P. Emma, R. Akre, J. Arthur, R. Bionta, C. Bostedt, J. Bozek, A. Brachmann, P. Bucksbaum, R. Coffee, F.-J Decker, Y. Ding, D. Dowell, S. Edstrom, A. Fisher, J. Frisch, S. Gilevich, J. Hastings, G. Hays, and P. Hering, First lasing and operation of an ångstrom-wavelength free-electron laser, Nat. Photon. **4**, 641 (2010).

[6] E. Allaria, P. Cinquegrana, S. Cleva, D. Cocco, M. Cornacchia, P. Craievich, I. Cudin, G. D'Auria, M. Dal Forno, M. Danailov, R. De Monte, G. Ninno, P. Delgiusto, A. Demidovich, S. Di Mitri, B. Diviacco, A. Fabris, R. Fabris, W. Fawley, and M. Zangrando, Highly coherent and stable pulses from the Fermi seeded free-electron laser in the extreme ultraviolet, Nat. Photon. **6**, 699 (2012).

[7] D. Gauthier, P. R. Ribič, G. De Ninno, E. Allaria, P. Cinquegrana, M. B. Danailov, A. Demidovich, E. Ferrari, L. Giannessi, B. Mahieu, and G. Penco, Spectrotemporal shaping of seeded free-electron laser pulses, Phys. Rev. Lett. **115**, 114801 (2015).

[8] R. Kienberger, E. Goulielmakis, M. Uiberacker, A. Baltuska, V. Yakovlev, F. Bammer, A. Scrinzi, T. Westerwalbesloh, U. Kleineberg, U. Heinzmann, M. Drescher, and F. Krausz, Atomic transient recorder, Nature (London) **427**, 817 (2004).

[9] J. Su, H. Ni, A. Jaroń-Becker, and A. Becker, Time delays in two-photon ionization, Phys. Rev. Lett. **113**, 263002 (2014).

[10] M. Swoboda, T. Fordell, K. Klünder, J. M. Dahlström, M. Miranda, C. Buth, K. J. Schafer, J. Mauritsson, A. L'Huillier, and M. Gisselbrecht, Phase measurement of resonant two-photon ionization in helium, Phys. Rev. Lett. **104**, 103003 (2010).

[11] A. S. Kheifets, Strongly resonant reconstruction of attosecond beating by interference of two-photon transitions on lithium, Phys. Rev. A **104**, L021103 (2021).

[12] A. Kheifets, Revealing the target electronic structure with under-threshold RABBITT, Atoms **9**, 66 (2021).

[13] A. S. Kheifets and A. W. Bray, RABBITT phase transition across the ionization threshold, Phys. Rev. A **103**, L011101 (2021).

[14] X. Yu, M. Han, Z. Guo, and Y. Liu, Intrinsic resonant photoionization time delay of hydrogen atoms probed with attosecond beating of asymmetrical photon transitions, Phys. Rev. A **104**, 063108 (2021).

[15] L. Neoričić, D. Busto, H. Laurell, R. Weissenbilder, M. Ammitzböll, S. Luo, J. Peschel, H. Wikmark Kreuger, J. Lahl, S. Maclot, R. Squibb, S. Zhong, P. Eng-Johnsson, C. Arnold, R. Feifel, M. Gisselbrecht, E. Lindroth, and A. L'Huillier, Resonant two-photon ionization of helium atoms studied by attosecond interferometry, Front. Phys. **10**, 964586 (2022).

[16] A. Autuori, D. Platzer, M. Lejman, G. Gallician, L. Maëder, A. Covolo, L. Bosse, M. Dalui, D. Bresteau, J.-F. Hergott, O. Tcherbakoff, H. Marroux, V. Loriot, F. lépine, L. Poisson, R. Taieb, J. Caillat, and P. Salieres, Anisotropic dynamics of two-photon ionization: An attosecond movie of photoemission, Sci. Adv. **8**, eabl7594 (2022).

[17] L. Drescher, T. Witting, O. Kornilov, and M. J. J. Vrakking, Phase dependence of resonant and antiresonant two-photon excitations, Phys. Rev. A **105**, L011101 (2022).

[18] Y. Liao, Y. Zhou, L.-W. Pi, J. Liang, Q. Ke, Y. Zhao, M. Li, and P. Lu, Reconstruction of attosecond beating by interference of two-photon transitions on the lithium atom with Rabi oscillations, Phys. Rev. A **105**, 063110 (2022).

[19] P.-M. Paul, E. Toma, P. Breger, G. Mullot, F. Auge, P. Balcou, H. Muller, and P. Agostini, Observation of a train of attosecond pulses from high harmonic generation, Science **292**, 1689 (2001).

[20] E. P. Wigner, Lower limit for the energy derivative of the scattering phase shift, Phys. Rev. **98**, 145 (1955).

[21] S. Heuser, Á. Jiménez Galán, C. Cirelli, C. Marante, M. Sabbar, R. Boge, M. Lucchini, L. Gallmann, I. Ivanov, A. S. Kheifets, J. M. Dahlström, E. Lindroth, L. Argenti, F. Martín, and U. Keller, Angular dependence of photoemission time delay in helium, Phys. Rev. A **94**, 063409 (2016).

[22] A. W. Bray, F. Naseem, and A. S. Kheifets, Simulation of angular-resolved RABBITT measurements in noble-gas atoms, Phys. Rev. A **97**, 063404 (2018).

[23] I. A. Ivanov and A. S. Kheifets, Angle-dependent time delay in two-color XUV+IR photoemission of He and Ne, Phys. Rev. A **96**, 013408 (2017).

[24] D. M. Villeneuve, P. Hockett, M. Vrakking, and H. Niikura, Coherent imaging of an attosecond electron wave packet, Science **356**, 1150 (2017).

[25] G. Zhenning, P. Ge, Y. Fang, Y. Dou, Y. Yu, J. Wang, Q. Gong, and Y. Liu, Probing molecular frame Wigner time delay and electron wavepacket phase structure of CO molecule, Ultrafast Sci. **2022**, 9802917 (2022).

[26] J. Dahlström, D. Guenot, K. Klünder, M. Gisselbrecht, J. Mauritsson, A. L'Huillier, A. Maquet, and R. Taieb, Theory of attosecond delays in laser-assisted photoionization, Chem. Phys. **414**, 53 (2011).

[27] J. Dahlström, A. L'Huillier, and A. Maquet, Introduction to attosecond delays in photoionization, J. Phys. B **45**, 183001 (2012).

[28] K. L. Ishikawa and K. Ueda, Competition of resonant and nonresonant paths in resonance-enhanced two-photon single ionization of He by an ultrashort extreme-ultraviolet pulse, Phys. Rev. Lett. **108**, 033003 (2012).

[29] K. L. Ishikawa and K. Ueda, Photoelectron angular distribution and phase in two-photon single ionization of H and He by a femtosecond and attosecond extreme-ultraviolet pulse, Appl. Sci. **3**, 189 (2013).

[30] M. Vacher, R. Gaillac, A. Maquet, R. Taieb, and J. Caillat, Transition dynamics in two-photon ionisation, J. Opt. **19**, 114011 (2017).

[31] Á. Jiménez-Galán, F. Martín, and L. Argenti, Two-photon finite-pulse model for resonant transitions in attosecond experiments, Phys. Rev. A **93**, 023429 (2016).

[32] N. Dudovich, B. Dayan, S. M. Gallagher Faeder, and Y. Silberberg, Transform-limited pulses are not optimal for resonant multiphoton transitions, Phys. Rev. Lett. **86**, 47 (2001).

[33] L. H. Haber, B. Doughty, and S. R. Leone, Continuum phase shifts and partial cross sections for photoionization from excited states of atomic helium measured by high-order harmonic optical pump-probe velocity map imaging, Phys. Rev. A **79**, 031401(R) (2009).

[34] R. Ma *et al.*, Photoelectron angular distributions for the two-photon ionization of helium by ultrashort extreme ultraviolet free-electron laser pulses, J. Phys. B **46**, 164018 (2013).

[35] J. Liang, M. Han, Y. Liao, J.-B. Ji, C. Leung, W.-C. Jiang, K. Ueda, Y. Zhou, P. Lu, and H. J. Wörner, Attosecond-resolved non-dipole photoionization dynamics, Nat. Photon. (2024), doi:10.1038/s41566-023-01349-z.

[36] S. H. Autler and C. H. Townes, Stark effect in rapidly varying fields, Phys. Rev. **100**, 703 (1955).

[37] B. Walker, M. Kaluža, B. Sheehy, P. Agostini, and L. F. DiMauro, Observation of continuum-continuum Autler-Townes splitting, Phys. Rev. Lett. **75**, 633 (1995).

[38] J. Qi, G. Lazarov, X. Wang, L. Li, L. M. Narducci, A. M. Lyyra, and F. C. Spano, Autler-Townes splitting in molecular lithium: Prospects for all-optical alignment of nonpolar molecules, Phys. Rev. Lett. **83**, 288 (1999).

[39] E. H. Ahmed, S. Ingram, T. Kirova, O. Salihoglu, J. Huennekens, J. Qi, Y. Guan, and A. M. Lyyra, Quantum control of the spin-orbit interaction using the Autler-Townes effect, Phys. Rev. Lett. **107**, 163601 (2011).

[40] M. G. Bustamante, V. D. Rodríguez, and R. O. Barrachina, Secondary peaks in the atomic ionization by a resonant laser pulse, J. Phys.: Conf. Ser. **397**, 012014 (2012).

[41] W.-C. Jiang, H. Liang, S. Wang, L.-Y. Peng, and J. Burgdörfer, Enhancing Autler-Townes splittings by ultrafast XUV pulses, Phys. Rev. Res. **3**, L032052 (2021).

[42] S. Nandi *et al.*, Observation of Rabi dynamics with a short-wavelength free-electron laser, Nature (London) **608**, 488 (2022).

[43] P. L. Knight and P. W. Milonni, The Rabi frequency in optical spectra, Phys. Rep. **66**, 21 (1980).

[44] M. Di Fraia *et al.*, Complete characterization of phase and amplitude of bichromatic extreme ultraviolet light, Phys. Rev. Lett. **123**, 213904 (2019).

[45] D. You *et al.*, New method for measuring angle-resolved phases in photoemission, Phys. Rev. X **10**, 031070 (2020).

[46] A. N. Grum-Grzhimailo, E. V. Gryzlova, E. I. Staroselskaya, J. Venzke, and K. Bartschat, Interfering one-photon and two-photon ionization by femtosecond VUV pulses in the region of an intermediate resonance, Phys. Rev. A **91**, 063418 (2015).

[47] N. Douguet, A. N. Grum-Grzhimailo, E. V. Gryzlova, E. I. Staroselskaya, J. Venzke, and K. Bartschat, Photoelectron angular distributions in bichromatic atomic ionization induced by circularly polarized VUV femtosecond pulses, Phys. Rev. A **93**, 033402 (2016).

[48] N. Douguet, E. Gryzlova, E. Staroselskaya, K. Bartschat, and A. Grum-Grzhimailo, Photoelectron angular distribution in two-pathway ionization of neon with femtosecond XUV pulses, Eur. Phys. J. D **71**, 105 (2017).

[49] E. V. Gryzlova, A. N. Grum-Grzhimailo, E. I. Staroselskaya, N. Douguet, and K. Bartschat, Quantum coherent control of the

photoelectron angular distribution in bichromatic-field ionization of atomic neon, Phys. Rev. A **97**, 013420 (2018).

[50] E. V. Gryzlova *et al.*, Influence of an atomic resonance on the coherent control of the photoionization process, Phys. Rev. Res. **4**, 033231 (2022).

[51] A. Tóth and A. Csehi, Probing strong-field two-photon transitions through dynamic interference, J. Phys. B **54**, 035005 (2021).

[52] X. Zhang, Y. Zhou, Y. Liao, Y. Chen, J. Liang, Q. Ke, M. Li, A. Csehi, and P. Lu, Effect of nonresonant states in near-resonant two-photon ionization of hydrogen, Phys. Rev. A **106**, 063114 (2022).

[53] J. Liang, Y. Zhou, Y. Liao, W.-C. Jiang, M. Li, and P. Lu, Direct visualization of deforming atomic wavefunction in ultraintense high-frequency laser pulses, Ultrafast Sci. **2022**, 9842716 (2022).

[54] T. N. Rescigno and C. W. McCurdy, Numerical grid methods for quantum-mechanical scattering problems, Phys. Rev. A **62**, 032706 (2000).

[55] W.-C. Jiang and X. Tian, Efficient split-Lanczos propagator for strong-field ionization of atoms, Opt. Express **25**, 26832 (2017).

[56] D. G. Arbó, J. E. Miraglia, M. S. Gravielle, K. Schiessl, E. Persson, and J. Burgdörfer, Coulomb-Volkov approximation for near-threshold ionization by short laser pulses, Phys. Rev. A **77**, 013401 (2008).

[57] T. Pfeifer, Y. Jiang, S. Düsterer, R. Moshammer, and J. Ullrich, Partial-coherence method to model experimental free-electron laser pulse statistics, Opt. Lett. **35**, 3441 (2010).

[58] A. F. Starace, Atomic photoionization, in *Fundamental Processes in Energetic Atomic Collisions* (Springer, New York, 1983), pp. 69–110.

[59] D. H. Oza, Phase shifts and resonances for electron scattering by He^+ below the $N = 2$ threshold, Phys. Rev. A **33**, 824 (1986).

[60] T. Gien, Accurate calculation of phase shifts for positron-He+ collisions, J. Phys. B **34**, L535 (2001).